Temporal evolution of the vibrational excitation within the $X\,^1\Sigma_g^+$ state of N_2 in the positive column of a pulsed electric discharge

Alexander Ershov, Edward Augustyniak, and Jacek Borysow
Department of Physics, Michigan Technological University, Houghton, Michigan 49931
(Received 18 April 1994)

The vibrational excitation to $v = 1$ level of the ground electronic state $X\,^1\Sigma_g^+$ of nitrogen was measured in a positive column during the 40-μs pulsed electric discharge, and in the afterglow. The discharge was operating at 6 Torr pressure and at current densities in the range 0.7–6.4 A/cm^2. Temporal evolution of vibrational excitation was measured using coherent anti-Stokes Raman scattering (CARS). Vibrational temperatures were found to range from 700 to 4000 K. The results are in fair agreement with model calculations based on energy transfer to vibrational excitation. Vibrational temperatures of the $X\,^1\Sigma_g^+$ state, obtained from direct CARS measurements, were up to a factor of 3 below those deduced from the second positive system emission.

PACS number(s): 34.80.Gs, 34.50.Ez, 42.65.Dr

I. INTRODUCTION

It is known that vibrational excitation of the ground electronic state of nitrogen $X\,^1\Sigma_g^+$ (for brevity denoted by X) in positive-column discharges is a main sink and reservoir of energy [1]. Therefore many processes in nitrogen pulsed discharges are strongly affected by vibrational population of the ground electronic state. For example, vibrationally hot nitrogen molecules can significantly raise electron temperature [1]. This affects the rate of loss of ions through processes like electron-ion recombination and ambipolar diffusion, particularly in the afterglow. The vibrational distribution influences dissociation rate. The so called pure vibrational mechanism is claimed to be the most efficient channel of N_2 dissociation at moderate values of the reduced electric field E/N [1,2]. The density of atoms strongly affects lifetimes of electronic metastable states of nitrogen molecule [3,4]. The present work is a continuation of our previous experiments aimed at study of metastable $A'\,^5\Sigma_g^+$ and $A\,^3\Sigma_u^+$ states of nitrogen in the high current pulsed discharges [5,4].

In order to analyze the physics of these types of discharges in N_2 one needs to make simultaneous determination of various parameters which include electric field transients, $N_2{}^+$ densities, the gas temperature, N atoms, $N_4{}^+$ ion densities, and the vibrational temperature of molecules in the X state. The first three measurements were recently reported [6]. Although several experimental and theoretical investigations of vibrational excitation and relaxation in low pressure nitrogen glow discharges have been undertaken, only scarce information can be found for nonflow pulsed discharges in μs scale [7–9]. Virtually no experiments verified the dynamics of vibrational excitation in a positive column of a pulsed discharge.

In this paper we report direct measurements of relative population of the two lowest vibrational levels of the X state in a positive column of the high-current pulsed discharge using nonlinear Raman spectroscopy. Experimental results are compared with calculations based on energy balance of electron impact excitation. Additionally we show comparison between vibrational temperatures obtained from an indirect (but widely used) method based on the observation of relative emission intensities within $C\,^3\Pi_u \rightarrow B\,^3\Pi_g$ system [10] and direct measurements based on the nonlinear Raman spectroscopy within the X state.

Nonlinear Raman spectroscopy has been successfully applied for diagnosis of internal energy distribution, e.g. [11–13]. For our studies we applied coherent anti-Stokes Raman scattering (CARS) spectroscopy. The description of this technique and its application to gases has been given in many publications; see for example [14,15]. This technique offers high sensitivity. The time resolution is in the order of the laser pulse duration and spatial resolution is limited to the size of the focused laser beams.

II. EXPERIMENT

A. Discharge conditions

The positive column of a pure nitrogen pulsed discharge was formed in a 10-cm-long, 0.6-cm-i.d. Pyrex tube with hollow aluminum electrodes and quartz windows at the ends.

The discharge was operated by applying high voltage (up to 2000 V) negative pulses to the cathode. These pulses were added to the dc voltage (about 1500 V) of the same polarity. A highly reproducible pulsed discharge of 40-μs duration was obtained that way. The discharge was synchronized to the pulsed laser, both operating at the repetition rate of 10 Hz.

The peak currents were from 0.2 to 1.8 A, corresponding to current densities of 0.7 to 6.4 A/cm^2 and were limited by a variable resistor. They were reproducible within 5% accuracy. The derived electron densities have varied from 6×10^{11} to 6×10^{12} cm^{-3}. The current wave-

form was close to rectangular pulse shape of 40-μs length with raise and turn off times of 1 μs.

Experiments were carried out at the gas pressure of 6 Torr. This was the lowest pressure which offered satisfactory signal-to-noise ratio of the CARS signal from the $v = 1$ level. Pressure was measured by means of the convectron gauge calibrated against the capacitance manometer accurate to 5×10^{-3} Torr. The system was pumped down to 6×10^{-3} Torr between runs. The gas was rated to be 99.9995% pure nitrogen and was used without further purification.

The CARS signal from the $X(v = 0)$ state appeared to be constant within experimental error after cessation of the active discharge in the time interval 10 ms–5 min, when recombination of atomic nitrogen was expected. This proved that dissociation of molecular nitrogen was less than about 5% under conditions of our discharge. No obvious inhomogeneities in the positive column were observed.

B. Laser system

The experimental setup used in our laboratory is shown in Fig. 1. Second harmonic of the Nd:YAG laser (532 nm) and the dye laser operating near 607 nm served as a pump ω_L and Stocks ω_S beams, respectively. The mixture of Rhodamine 610 and Rhodamine 640 was used to generate radiation between 607 and 604 nm. The dye laser consisted of an oscillator, preamplifier, and final amplifier. It was tuned to match the frequency difference $\omega_L - \omega_S$ to the (0-1) vibrational frequency ω_{vib} of the $X\,^1\Sigma_g^+$ state of nitrogen. As a result of nonlinear interaction, the anti-Stokes Raman signal at frequency

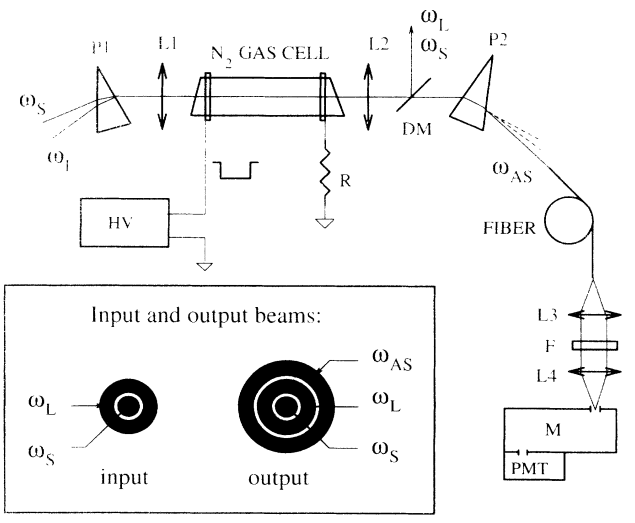

FIG. 1. Experimental apparatus; ω_S, ω_L, and ω_{AS}: Stokes, pump, and anti-Stokes beams; P_1, P_2: prisms; L_1, L_2, L_3, and L_4: quartz lenses; DM: dichroic mirror; F: filter; M: monochromator; PMT: photomultiplier; HV: high voltage modulator; R: resistor. The inset shows cross section of the input and output beams.

$\omega_{AS} = 2\omega_L - \omega_S$ was generated in the vicinity of 473 nm.

The 30 GHz linewidth of our YAG laser set the limit on the resolution of the CARS spectrometer. It significantly exceeded the Doppler limited Raman linewidth at 400 K (typical gas temperature under our conditions [4]). This resolution was insufficient to observe single rotovibrational lines. Both beams were linearly polarized in the same direction.

In order to eliminate signal from outside the discharge sample we chose the unstable-resonator spatially enhanced detection (USED) CARS geometry [16]. In this arrangement the Stokes laser beam is traveling inside the "doughnut" shaped YAG laser, preventing overlapping of the two beams outside the discharge region (see Fig. 1). No CARS signal from $X\,^1\Sigma_g^+(v = 0)$ state of N_2 could be detected when the sample was pumped down to its background pressure. The USED CARS geometry improves also the longitudinal spatial resolution very much like the BOXCARS technique [16]. We estimate that 90% of the signal was generated within the range of 1 cm length in the middle of a positive column.

The prism P_1 (see Fig. 1) was used to bring the laser and the Stokes beams into collinear configuration. According to our estimates, during 1-nm scan (range required to measure signals from the first two vibrational levels of $X\,^1\Sigma_g^+$) the misalignment of the beams due to dispersion of the prism distorted the ratio of CARS signals from $v = 1$ and $v = 0$ by less than 5%. We considered this error to be small in comparison with laser power and polarization fluctuations. Similarly, no correction needed to be taken for the changing laser power during the scan of the dye laser over such a short distance.

Following the prism P_1 (Fig. 1), laser beams were focused by the 25-cm focal length lens L_1 on the gas cell. Lens L_2 recollimated the signal, laser, and Stokes beams behind the discharge tube. The dichroic mirror DM rejected 532 and 607 nm lasers, passing anti-Stokes laser generated in nitrogen at 473 nm. The prism P_2 separated spatially the unrejected lasers from the CARS signal. The CARS signal was focused onto the optical fiber, passed through 10-nm bandwidth interference filter F, and imaged at the entrance slit of the monochromator.

A photomultiplier was used to measure the CARS signal on the output of the monochromator. The entire system behind the discharge tube, consisting of a dichroic mirror, prism, fiber, interference filter, and monochromator, served to reject lasers and pass the CARS signal to the photomultiplier.

The problem which we were unable to overcome was misalignment of laser beams as the discharge progressed in time. We believe the effect was due to sudden changes of the refractive index as a result of acoustic waves created by the discharge. This effect starts to be significant approximately 10 μs after beginning of the discharge and vanishes about 1 ms after the discharge. Nonresonant index of refraction is only weekly frequency dependent. Therefore, we believe it did not affect the vibrational temperature transients deduced from relative CARS signals from different vibrational levels. The misalignment of laser beams, following the discharge, limited our abil-

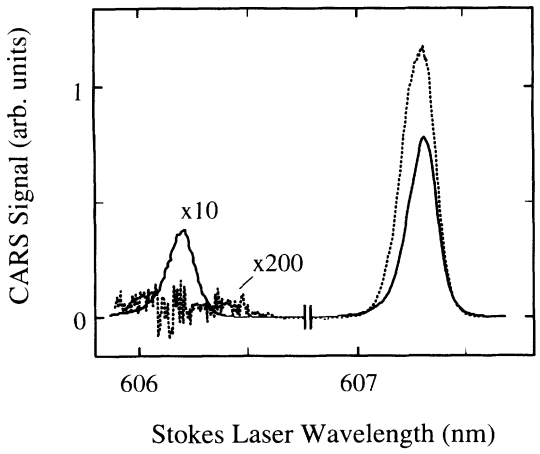

FIG. 2. CARS spectra versus Stokes laser wavelength. Solid line: 17.5 μs after the beginning of the 0.3 A pulse. Dotted line: cold spectrum taken 100 ms in the afterglow. The two traces are drawn in different scales. Note also the change of scale to the left of the marker.

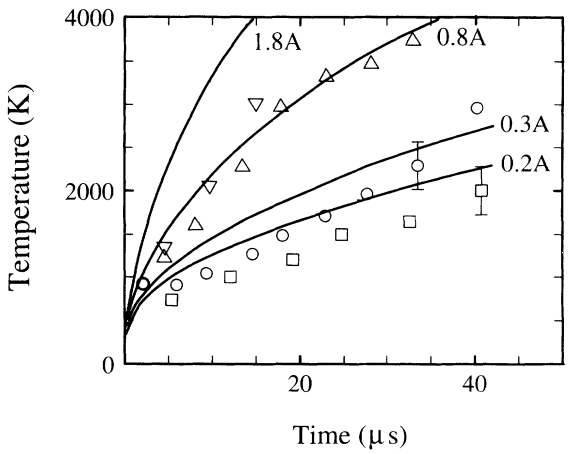

FIG. 3. Vibrational temperature of the X state measured by CARS for different peak currents, 40 μs pulse and 6 Torr pressure; □, 0.2 A; ○, 0.3 A; △, 0.8 A; ▽, 1.8 A. Experimental errors shown for two data points. Calculated temperatures represented by solid curves.

ity to measure the vibrational excitation transients for a wider range of currents and time durations of discharge pulses.

In the course of the experiment the CARS signal was measured as a function of the scanning Stokes laser frequency. These measurements were taken at different times with respect to the beginning of the discharge pulse. Both regions, during the current pulse and afterglow, were examined. All measurements were done for $v' = 2 \leftarrow v'' = 1$ and $v' = 1 \leftarrow v'' = 0$ rotationally unresolved Q-branch transitions. The typical CARS spectra are presented in Fig. 2. They are not corrected for the spectral response of the interference filter and monochromator. The solid line represents the CARS signal from the vibrationally excited nitrogen (temperature 1500 K). The dotted trace was taken with the vibrationally cold gas in the afterglow. At this time only the $v = 0$ band is clearly visible. The boxcar gate was set to 100 ns and the signal was averaged over 30 laser shots.

III. VIBRATIONAL DISTRIBUTION OF THE $X\,^1\Sigma_g^+$ STATE OF N_2

A. Direct measurements; CARS

We derived the number density ratio $N_{v=1}/N_{v=0}$ of the first two vibrational levels of the $X\,^1\Sigma_g^+$ electronic state following the method described in Ref. [13]. Additionally, we assumed that rotational distribution within both vibrational bands is the same. The 0-1 temperature was calculated as $kT_v = \epsilon/\ln(N_{v=0}/N_{v=1})$, where ϵ is a vibrational spacing between $v = 0$ and $v = 1$ levels.

The deduced vibrational temperatures for peak currents ranging from 0.2 to 1.8 A as a function of time are presented in Fig. 3. The acoustic effects described in the preceding section limited our measurements at high currents to times below 15 μs after the beginning of the discharge pulse. The solid curves in Fig. 3 represent model calculations for each data set.

Energy balance of electron impact reaction was used to calculate the energy input into the vibrational degree of freedom [8]:

$$\frac{d\mathcal{E}}{dt} = j\frac{E}{N}f_v - \frac{\mathcal{E}}{\tau}, \tag{1}$$

where $\mathcal{E}$ is the average vibrational energy per molecule, j is the measured current density, E/N is the reduced electric field, f_v is the fractional power input to vibrational excitation [1], and τ is the relaxation time due to electron deexcitation [8,1].

The time dependence of E/N was concluded from Borysow and Phelps [6] measurements using the NR scaling to account for our different pressure and tube radius. The estimated error for the resulting E/N transients is in the range of 20%. For peak currents 0.2 and 0.3 A the calculated vibrational temperatures are few hundred degrees higher than temperatures from the CARS measurements. At 0.8 A the agreement is strikingly good. The measured temperatures for current of 1.8 A appeared to be significantly lower than the calculated values. All model calculations and experimental derivations were done under assumption of the Boltzmann distribution of $(X\,^1\Sigma_g^+, v)$ states.

The average vibrational energy $\mathcal{E}$ is proportional to $N_{v=1}/(N_{v=0} - N_{v=1})$. The rate of change of $\mathcal{E}$ in the afterglow is shown in Fig. 4. Vibrational relaxation time appeared to be 3 ms at the pressure of 6 Torr. Since this time is much shorter than the afterglow period at the repetition rate of 10 Hz, the integration of Eq. (1) starts from $\mathcal{E} = 0$ for every discharge cycle (no accumulation of vibrational energy).

V-T relaxation time is 6 s atm [17], which corresponds to about 10 min for our pressure. Therefore, the only

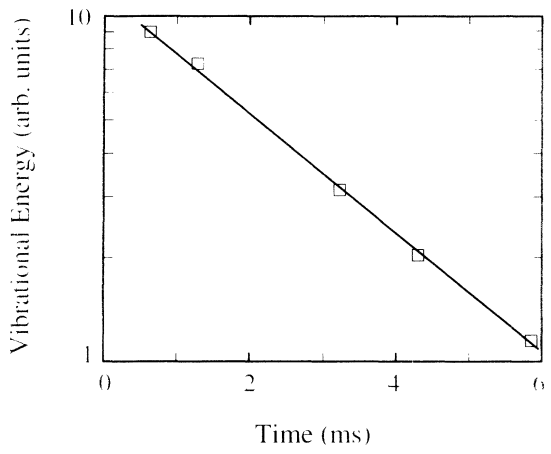

FIG. 4. Relaxation of the mean vibrational energy per molecule in the afterglow; time is measured from the discharge turn off.

mechanisms of vibrational cooling between the pulses are deexcitation on walls and diffusion of vibrationally hot molecules out of the discharge tube. Calculations of longitudinal diffusion in our tube at 6 Torr pressure showed that the density of vibrationally hot molecules in the central region of the tube was diminishing by no more than 5% due to this process during 100 ms of the afterglow period. Thus diffusion in the radial direction is much more important, yielding the afterglow deexcitation time $2R/(\gamma w) = 3$ ms, where w is the average speed of molecules and γ is the wall deexcitation coefficient. In our case, we get $\gamma = 4 \times 10^{-3}$ which is by a factor of 3–10 higher than other reported γ values for untreated Pyrex surfaces [18].

The details of calculations of vibrational excitation in nitrogen pulsed discharges were presented in our previous paper [4].

B. Indirect measurements; $C\,^3\Pi_u \rightarrow B\,^3\Pi_g$ emission

We have compared the 0-1 vibrational temperature obtained from CARS measurements with the indirect method based on measurement of vibrational distribution of the $C\,^3\Pi_u$ state. Passive emission from the second positive system of nitrogen $C\,^3\Pi_u(v') \rightarrow B\,^3\Pi_g(v'')$, $v'' - v' = 2$ (for $v' = 0,1,2,3,4$) was observed with the apparatus shown in Fig. 1 with all the filters used in the CARS experiment removed. Emission was collected by $f/1.1$ quartz lens and imaged onto the 1-mm-diam quartz optical fiber. Another end of the fiber was imaged by a system of two quartz lenses onto the entrance slit of the 0.5-m scanning monochromator-photomultiplier system. The spectral resolution of the monochromator was set to 1 nm. The signal processing electronics was identical to the one used in the CARS experiment. For a purpose of derivation of the $C\,^3\Pi_u$ state temperature from $C \rightarrow B$ emission we used spectroscopic data from Ref. [19].

The simplest method of inferring the X state temperature from the measured C state temperature is based on the following assumptions: (1) The C state is populated only by the electron impact from the X state. (2) Electron impact favors "vertical" transitions ruled by the Franck-Condon principle. (3) Short radiative lifetime of the C state prevents redistribution of vibrational energy. The reactions describing these processes are

$$N_2(X,v'') + e \xrightarrow{k^{XC}_{v''v'}} N_2(C,v') + e,$$

$$N_2(C,v') \xrightarrow{A^{CB}_{v'v}} N_2(B,v) + h\nu,$$

where $k^{XC}_{v''v'}$ are v-specific rate coefficients and $A^{CB}_{v'v}$ are appropriate Einstein coefficients [19].

The above assumptions formed a basis for models of dc discharges used in Refs. [10,22] relating measured vibrational distribution of the C state to the vibrational excitation of the X state. The rate of change of the C state distribution and its relation to the vibrational distribution of the X state is described by the set of rate equations below:

$$\frac{d[N_2(C,v')]}{dt} = n_e(t) \sum_{v''} R^{XC}_{v''v'} - [N_2(C,v')]/\tau_{v'}, \quad (2)$$

where $R^{XC}_{v''v'} = [N_2(X,v'')]k^{XC}_{v''v'}$ are partial rates, $[N_2(C,v')]$, $[N_2(X,v'')]$ are time-dependent densities of molecules in respective electronic-vibrational states, $\tau_{v'} = (\sum_v A^{CB}_{v'v})^{-1}$ denotes radiative lifetimes of $N_2(C,v')$, and $n_e(t)$ is the electron density inferred from a discharge current. Partial rate constants $k^{XC}_{v''v'}$ were estimated from the total rate of the $N_2(X) + e \rightarrow N_2(C) + e$ reaction [1] using methods of [20,21]. Coefficients $k^{XC}_{v''v'}$ are implicit functions of time: they depend on the reduced electric field E/N, which is evolving during the discharge.

The calculated C state population follows closely Boltzmann-type distribution provided the same is true for the X state. There is no significant time lag between the C and X states vibrational distributions due to the short radiative lifetime of the C state.

The X state temperatures, deduced from this simple model and from the C state measurements, exceeded significantly directly measured values. Therefore, we have extended the above model and included other processes populating the C state. Three possible mechanisms where considered: (1) collisional cascading from the $E\,^3\Sigma^+_g$ state; (2) energy pooling reaction from the $A\,^3\Sigma^+_u$ state; and (3) electron impact excitation from electronic states other than X, e.g., $A\,^3\Sigma^+_u$.

It is known that the C state is also populated by collisional cascading from the high lying triplet state $E\,^3\Sigma^+_g$ [23]. The E state is produced during the discharge by an electron impact at a rate about one order of magnitude lower than the C state [1]. It lives relatively long and is strongly collisionally coupled to the C state ($k^{EC} = 1.2 \times 10^{-10}$ cm^3/s) [23]. The following reactions were considered:

$$N_2(X, v'') + e \xrightarrow{k^{XE}_{v''v}} N_2(E, v) + e,$$

$$N_2(E, v) + N_2 \xrightarrow{k^{EC}_{vv'}} N_2(C, v') + N_2.$$

Partial rate coefficients $k^{XE}_{v''v}$ were found in the same way as $k^{XC}_{v''v'}$ constants, used in Eq. (2). The v-specific coupling rate constants $k^{EC}_{vv'}$ were evaluated using a model based on Franck-Condon overlap with minimum energy defect. This model, although failed for energy-pooling reactions [24], worked fairly good for $W\,^3\Delta_u$–$B\,^3\Pi_g$ collisional coupling [25]. In case of the E and C states, it predicts cascading mostly to $C\,^3\Pi_u(v = 3, 4)$. The E–C coupling is effective at the beginning of the discharge. As an example, the C temperatures are predicted to be higher by 500–800 K, due to cascading from the E state, for the X state temperatures below 2000 K.

Additional significant contribution to the C state population comes from the energy pooling reaction involving $A\,^3\Sigma^+_u$ metastables. It becomes important in later times of the discharge following the buildup of the A state. This reaction is described by

$$N_2(A, v' = 0, 1) + N_2(A, v'' = 0, 1) \longrightarrow N_2(C, v) + N_2.$$

The rate coefficients responsible for the process were taken from Ref. [24]. The population of the A state was estimated from our model which was verified experimentally under similar conditions [4,21]. Energy pooling process populates all v levels of the C state with similar rates, thus increasing the C apparent temperature. The inclusion of the A state energy pooling reduced the difference between the direct and indirect determination of X state temperature at the end of the discharge pulse, when the A state density is sufficiently high.

To our knowledge, there are no sufficient experimental data on electron impact excitation from the A or B states to the C state. Computational simulations of the $N_2(A) + e \rightarrow N_2(C) + e$ reaction, with the rate coefficient as for the $N_2(X) + e \rightarrow N_2(A) + e$ electron impact, yielded insignificant correction to the C state distributions under our conditions. We decided to ignore entirely this channel.

Comparison of the extended model prediction of the X state temperature, inferred from the C state distribution measurements with direct CARS results, is presented in Fig. 5. Generally, the C-based temperature is too high. The discrepancy is most pronounced at the beginning of the discharge pulse. This fact indicates that processes other than those analyzed here might contribute also to the C state excitation.

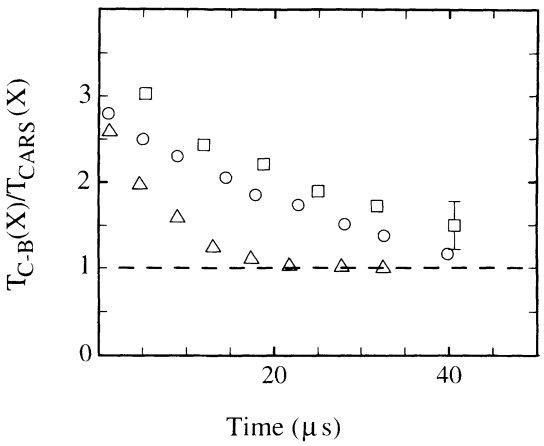

FIG. 5. Ratio of the X state vibrational temperatures during the discharge pulse: $T_{C\text{-}B}(X)$ derived from the C state distribution and $T_{CARS}(X)$ measured directly by CARS; □, 0.2 A; ○, 0.3 A; △, 0.8 A.

IV. CONCLUSIONS

We have measured the relative populations of the two lowest vibrational levels of the $X\,^1\Sigma^+_g$ state in a pure nitrogen pulsed discharge, as a function of time, by means of nonlinear Raman spectroscopy. Calculations of the population distribution, based on energy pumping into the vibrational degree of freedom, represent fairly the measured excitation within the X state. We have also shown that the derivation of vibrational temperature of the ground electronic state of nitrogen, from the second positive system emission in the pulsed nitrogen discharge, can be misleading. The attempt to find proper relation between vibrational excitations of the C and X states have failed, in particular at the beginning of the discharge.

ACKNOWLEDGMENTS

We would like to thank Dr. Art Phelps for inspiration to do this experiment and suggestions during his visit at Michigan Tech. The support of Dr. Sung Lee is gratefully appreciated.

[1] J. Loureiro and C. M. Ferreira, J. Phys. D **19**, 17 (1986).
[2] M. Capitelli, C. Gorse, and A. Ricard, J. Phys. Lett. (Paris) **43**, 417 (1982).
[3] L. G. Piper, J. Chem. Phys. **90**, 7087 (1989).
[4] E. Augustyniak and J. Borysow, J. Phys. D **27**, 652 (1994).
[5] C. Scripter, E. Augustyniak, and J. Borysow, Chem. Phys. Lett. **201**, 194 (1993).
[6] J. Borysow and A. V. Phelps, Phys. Rev. E **50**, 1399 (1994).
[7] S. K. Dhali and L. H. Low, J. Appl. Phys. **64**, 2917 (1988).

[8] O. Sahni and W. C. Jennings, J. Chem. Phys. **59**, 6070 (1973).
[9] J. P. Boeuf and E. E. Kunhardt, J. Appl. Phys. **60**, 915 (1986).
[10] S. Ono and S. Teii, J. Phys. D **16**, 163 (1983).
[11] R. J. Hall, Combust. Flame **35**, 47 (1979).
[12] A. C. Eckbreth, Combust. Flame **39**, 133 (1980).
[13] B. Massabieaux, G. Gousset, M. Lefebvre, and M. Péalat, J. Phys. (Paris) **48**, 1939 (1987).
[14] J. W. M. Tolles, J. W. Nibler, and A. B. Harvey, Appl. Spectrosc. **31**, 253 (1977).
[15] G. L. Eesley, *Coherent Raman Spectroscopy* (Pergamon Press, New York, 1981).
[16] A. C. Eckbreth, *Laser Diagnostics for Combustion Temperature and Species* (Abacus Press, Tunbridge Wells, Kent and Cambridge, MA, 1988).
[17] M. A. Kovacs, J. Quantum Electron. **QE-9**, 189 (1973).
[18] G. Black, H. Wise, S. Schechter, and R. L. Sharpless, J. Chem. Phys. **60**, 3526 (1974).
[19] F. R. Gilmore, R. R. Laher, and P. J. Espy, J. Phys. Chem. Ref. Data **21**, 1005 (1992).
[20] G. Cernogora *et al.*, J. Phys. B **17**, 4429 (1984).
[21] E. Augustyniak and J. Borysow (unpublished).
[22] A. D. Kosoruchkina, Sov. Phys. Tech. Phys. **20**, 676 (1976).
[23] D. J. Burns, D. E. Golden, and D. W. Galliardt, J. Chem. Phys. **65**, 2616 (1976).
[24] L. G. Piper, J. Chem. Phys. **88**, 231 (1988).
[25] A. Rotem and S. Rosenwaks, Opt. Eng. **22**, 564 (1983).

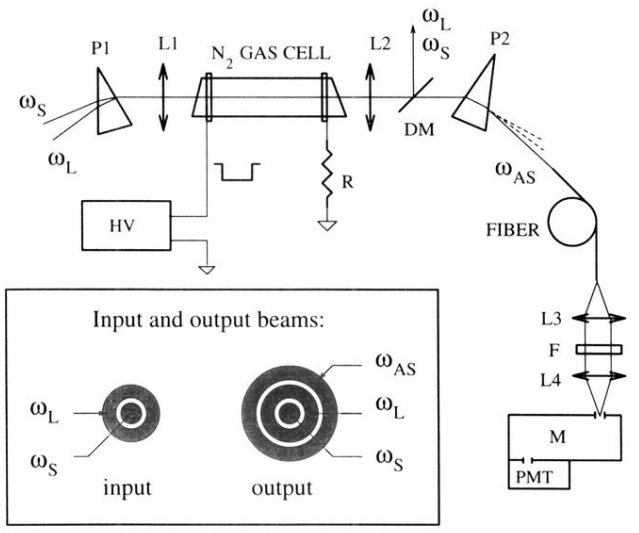

FIG. 1. Experimental apparatus; ω_S, ω_L, and ω_{AS}: Stokes, pump, and anti-Stokes beams; P_1, P_2: prisms; L_1, L_2, L_3, and L_4: quartz lenses; DM: dichroic mirror; F: filter; M: monochromator; PMT: photomultiplier; HV: high voltage modulator; R: resistor. The inset shows cross section of the input and output beams.